Available online at www.sciencedirect.com

ScienceDirect

IFAC Papers Online CONFERENCE PAPER ARCHIVE

IFAC PapersOnLine 55-21 (2022) 61–66

Extremum Seeking Control of a Flotation Circuit using Peak Air Recovery ⋆

D. A. Wepener * **J. D. le Roux** *,1 **I. K. Craig** *

* *Department of Electrical, Electronic and Computer Engineering, University of Pretoria, Pretoria, South Africa*

Abstract: A flotation circuit is simulated with an extremum seeking controller to keep the cells operating at the optimal operating point represented by peak air recovery. It is assumed that at this operating point, the froth layer is stabilised and the mineral recovery of the flotation cell is maximised resulting in optimal performance. The extremum seeking controller uses periodic perturbations in the aeration rate to steer the system through an unknown static map towards the peak in air recovery. The controller is able to find the peak air recovery operating point and track the point as it changes in the presence of external disturbances. The extremum seeking controller is ideally suited for model-independent long-term automated optimisation of a flotation circuit with a time-varying optimal operating point.

Keywords: Extremum seeking control, flotation circuit, peak air recovery, process control, optimisation

1. INTRODUCTION

The success of the flotation process is dependent on two main performance indicators: the mineral recovery and the product grade. The recovery is the fraction of the total amount of valuable minerals in the feed that are concentrated and the grade is the ratio of valuable minerals to gangue in the final product. The control objective of each flotation cell is to maximise grade and recovery, however, there is an inverse relationship between grade and recovery (Laurila et al., 2002). Flotation is a very complicated process with many different correlated variables that are affected by many variables. This makes the flotation process difficult to model accurately. Without an accurate model, advanced process control for flotation optimisation becomes challenging to implement and less effective (Quintanilla et al., 2021).

In the mineral processing industry, there is an incentive for improved optimisation control, especially long term automated advanced optimisation (Shean and Cilliers, 2011; Bergh and Yianatos, 2011). One possible solution for optimisation control of a flotation circuit is peak air recovery. Hadler and Cilliers (2009) report that the optimal performance of a flotation cell can be found by maximising the air recovery of the cell and operating at the peak air recovery point. At this optimal operating point, the froth is stabilised and the mineral recovery is maximised while the grade is kept at an acceptable level (Hadler et al., 2010).

Extremum seeking control (ESC) is an optimisation technique that maximises an objective function by exploring an unknown static map and steering the system towards the optimal operating condition (Krstić and Wang, 2000; Guay et al., 2015). Therefore, it is ideally suited to track and maintain peak air recovery for a flotation bank. Hence, in this paper, ESC is used to optimise a flotation circuit, similar to the optimisation performed for a grinding mill circuit by Ziolkowski et al. (2021).

The flotation process is described in Section 2, the process model description is given in Section 3, and air recovery is discussed in Section 4. In Section 5 an overview is given of ESC and in Section 6 the simulation setup and results are presented. In Section 7 the simulation results are discussed and the work is concluded in Section 8 by discussing the advantages and shortcomings of applying ESC to a flotation circuit.

2. PROCESS DESCRIPTION

The mineral processing chain consists of two main stages: the comminution stage and the separation stage. The run-of-mine ore first passes through the comminution stage, most often a grinding circuit, where the ore is ground into fine particles and mixed with water to form a slurry. The slurry then flows to the separation stage where the valuable minerals are separated from the gangue. There are many different types of separation circuits, but this study will focus on flotation only. In industry, flotation tanks are connected in flotation banks, with each bank performing a specific function. The functions of the flotations banks can be divided into three sections: rougher, scavenger and cleaner banks (Laurila et al., 2002). The flotation circuit used in this simulation study includes four flotation cells in the rougher section. The four cells are connected in series as shown in Fig. 1.

The slurry from the comminution stage flows into the first flotation cell with a flow rate, Q_{F_1}. The tailings flow rates of the slurry flowing out of the cells are given by

⋆ This work is based on research supported in part by the National Research Foundation of South Africa (Grant numbers, 130380 & 132380).

[1] Corresponding author, E-mail: derik.leroux@up.ac.za

10.1016/j.ifacol.2022.09.244

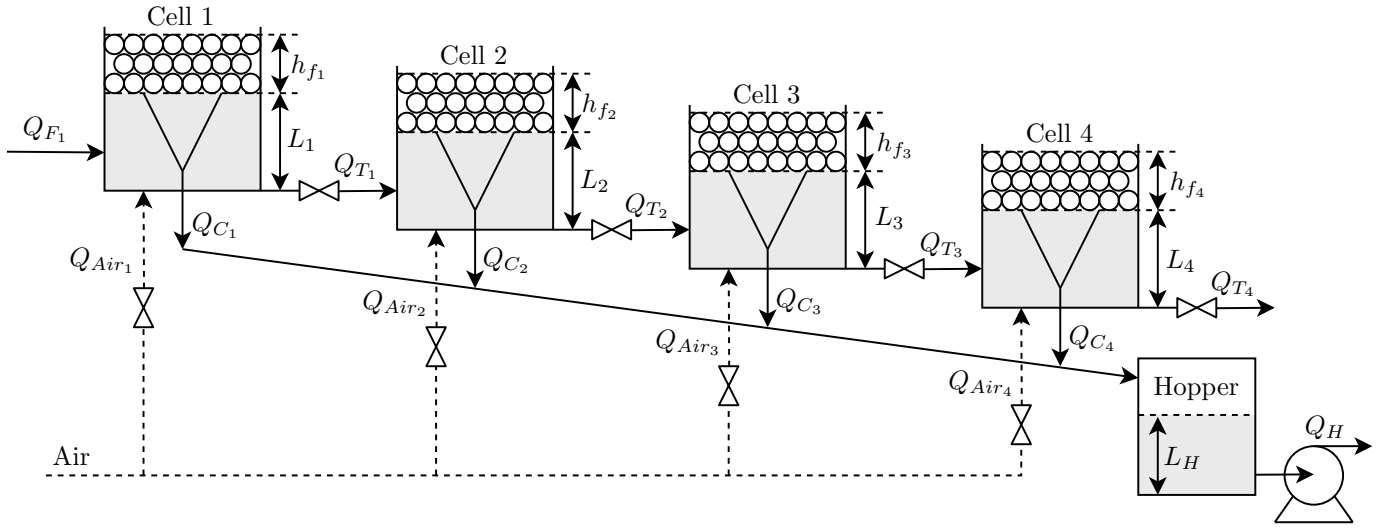

Fig. 1. Flotation circuit configuration (reproduced from Oosthuizen et al. (2021)).

Q_{T_k}, where k is the cell number. The aeration rate to each cell, Q_{Air_k}, gives the flow rate of air flowing into the cell and forming bubbles that rise through the slurry. The measurement of the aeration rate is the superficial gas velocity, J_{g_k}. As the air bubbles rise, the valuable mineral particles attach to the bubbles because of their hydrophobicity and collect in the froth layer at the top of the cell. The froth height is denoted by h_{f_k} while L_k is the pulp level in each cell. The air bubbles in the froth layer flow over the cell lip into the concentrate launder with flow rates, Q_{C_k}, and collect in the concentrate hopper. The slurry level in the hopper is given by L_H. From the hopper, the concentrate is pumped away for further processing with a flow rate of Q_H.

3. MODEL DESCRIPTION

The dynamic model of a four-cell flotation circuit given in Oosthuizen et al. (2021) is used to simulate the performance of the proposed controller. Each of the flotation cells has four states, the cell pulp level (L_k), the masses in the cell ($M_k^{i,j}$), the air recovery (α_k) and the top of froth bubble size (D_{BF_k}). The superscript, i, represents the different mineral species in the cell (gangue or valuable minerals) and j represents the different sub-classes within the mineral class for minerals with different flotabilities or sizes. In this simulation study the model is simplified to include only two mineral species, valuable minerals ($i = 0$) and gangue ($i = 1$). It is also assumed that there are no sub-classes and j will therefore be omitted. A comprehensive model description can be found in Oosthuizen et al. (2021).

The change in the pulp level of each cell is modelled using the volume balance in the cell,

$$\frac{d}{dt}L_k = \frac{Q_{F_k} - Q_{T_k} - Q_{C_k}}{A_k}, \tag{1}$$

where A_k is the surface area of cell k. The effect of a change in gas holdup on the change in level is not included in the model as it is relatively small compared to the effect of the flow rates and it changes on a much slower time-scale. The concentrate flow rate is calculated from the water recovery,

$$\frac{Q_{C_k}}{A_k} = \begin{cases} \dfrac{J_{g_k}^2 \lambda_{out}}{k_1}(1-\alpha_k)\alpha_k & 0 < \alpha_k < 0.5 \\ \dfrac{J_{g_k}^2 \lambda_{out}}{4k_1} & \alpha_k \geq 0.5 \end{cases}, \tag{2}$$

where J_{g_k} is the superficial gas velocity for cell k, and k_1 is a constant. The Plateau border length (λ_{out}) per volume of froth is inversely proportional to the square of the top of froth bubble diameter (D_{BF_k}),

$$\lambda_{out} \approx \frac{6.81}{D_{BF_k}^2}. \tag{3}$$

A mass balance is used to model the change in mass in each cell,

$$\frac{d}{dt}M_k^i = \dot{M}_{F_k}^i - \dot{M}_{T_k}^i - \dot{M}_{C_k}^i, \tag{4}$$

where $\dot{M}_{\Delta_k}^i$ is the mass flow rate associated with the feed ($\Delta = F$), tailings ($\Delta = T$) or concentrate ($\Delta = C$) of cell k. The tailings mass flow rate of cell k is the feed flow rate of the next cell, $\dot{M}_{F_{k+1}}^i = \dot{M}_{T_k}^i$, and is calculated by,

$$\dot{M}_{T_k}^i = \frac{M_k^i}{K_k A_k} Q_{T_k}. \tag{5}$$

True flotation is used to model the entrainment,

$$\dot{M}_{C_k}^i = K^i M_k^i S_{b_k} \alpha_k + Ent_{Frac}^i \frac{M_k^i}{A_k L_k} Q_{C_k}, \tag{6}$$

where K^i is a pseudo rate-constant, M_k^i is the mass of mineral i in cell k, S_{b_k} is the bubble surface area flux, and Ent_{Frac}^i is the mass that is entrained. The models for air recovery and the bubble size are empirical models derived by Oosthuizen et al. (2021) using industrial data. The change in air recovery is,

$$\frac{d}{dt}\alpha_k = \frac{\alpha_{SS} - \alpha_k}{\lambda_{air_k}}, \tag{7}$$

where λ_{air_k} is the average froth residence time,

$$\lambda_{air_k} = \frac{h_{f_k}}{J_{g_k}}. \tag{8}$$

The steady-state model of air recovery, α_{SS}, is given by,

$$\alpha_{SS} = K_{\alpha_{J_g}} \left(J_{g_k} - K_{\alpha_{J_{g0}}} \right)^2 + K_{\alpha_{h_f}} \left(h_{f_k} - K_{\alpha_{h_{f0}}} \right)^2. \tag{9}$$

The parameters, $K_{\alpha_{J_g}}$, $K_{\alpha_{J_{g0}}}$, $K_{\alpha_{h_f}}$ and $K_{\alpha_{h_{f0}}}$ are empirically fitted. The rate of change in bubble size is,

$$\frac{d}{dt}D_{BF_k} = \frac{K_{BS_{J_g}} J_{g_k} + K_{BS_\lambda}\lambda_{air_k} - D_{BF_k}}{\lambda_{air_k}}, \tag{10}$$

where $K_{BS_{J_g}}$ and K_{BS_λ} are empirically fitted parameters.

The concentrate hopper has two states, the hopper level (L_H) and the masses in the hopper (M_H^i). The state equations are,

$$\frac{d}{dt}L_H = \frac{Q_{C_1} + Q_{C_2} + Q_{C_3} + Q_{C_4} - Q_H}{A_k}, \tag{11}$$

$$\frac{d}{dt}M_H^i = \sum_{k=1}^{4} \dot{M}_{C_k}^i - \frac{M_H^i}{L_H A_H} Q_H. \tag{12}$$

The total mass pull rate of the hopper is given by,

$$\dot{M}_H^{Tot} = \left(\dot{M}_H^0 + \dot{M}_H^1\right) \frac{Q_H}{L_H A_H}. \tag{13}$$

The concentrate grade in the hopper is the ratio of the desired mass to the total mass in the hopper,

$$G_H = \frac{M_H^0}{M_H^0 + M_H^1}. \tag{14}$$

4. AIR RECOVERY

Air recovery is the fraction of the air that enters the flotation cell and overflows the lip of the cell in unburst bubbles. Air recovery can be seen as a measure of the stability of the froth in the flotation cell. Therefore, it is an indicator that can be used to evaluate the efficiency and performance of the flotation process.

The equation for air recovery is given by (Hadler et al., 2010),

$$\alpha = \frac{v_f \cdot h \cdot w}{Q_{Air}}, \tag{15}$$

where v_f is the overflow velocity of the froth, h is the overflow froth height above the cell lip, w is the overflow length, and Q_{Air} is the inlet air flow rate. On industrial flotation plants the air recovery can be measured with a froth vision system and laser-based froth height measurement (Shean et al., 2017; Phillpotts et al., 2020). For the simulation study a simplified air recovery model is used as given in (7)–(9).

Air recovery initially increases with an increase in aeration rate, but it reaches a peak after which a further increase in the aeration rate lowers the air recovery (Hadler and Cilliers, 2009; Hadler et al., 2010; Smith et al., 2010). At a low aeration rate, the bubbles rise slowly through the slurry to produce highly laden, well drained froths. The bubbles often collapse before overflowing the cell lip. The low aeration rate results in a high concentrate grade, but with low air recoveries and low mineral recoveries. At a high aeration rate, past the air recovery peak, the air moves fast through the cell and creates unstable bubbles that burst before they reach the top of the cell. These bubbles have a higher water content as the water becomes trapped between the bubbles which reduce the grade.

Fig. 2 shows the steady-state model simulation of air recovery for different aeration rates in the four cells using the model of Oosthuizen et al. (2021). As the aeration rate is increased, it is clear that the air recovery increases to a peak and then decreases again with a further increase in the aeration rate. Steady-state model simulations of the mineral recovery and grade, measured in the concentrate hopper, are shown in Fig. 3 and Fig. 4. In these figures, the inverse relationship between grade and recovery is demonstrated by the opposite gradients at most aeration rates.

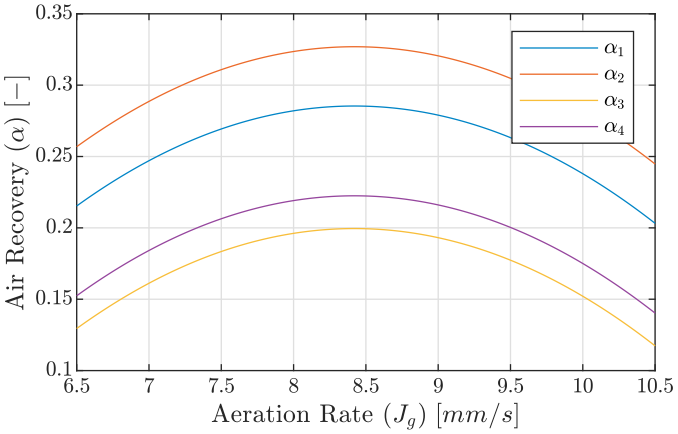

Fig. 2. Steady-state simulation of aeration rate and air recovery for each of the four flotation cells.

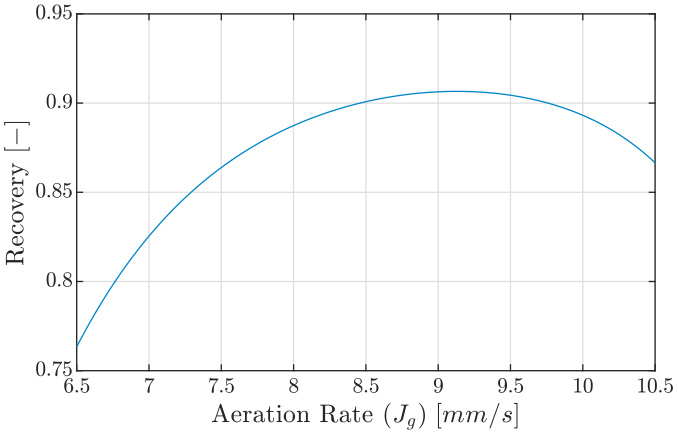

Fig. 3. Steady-state simulation of aeration rate and recovery measured in the hopper.

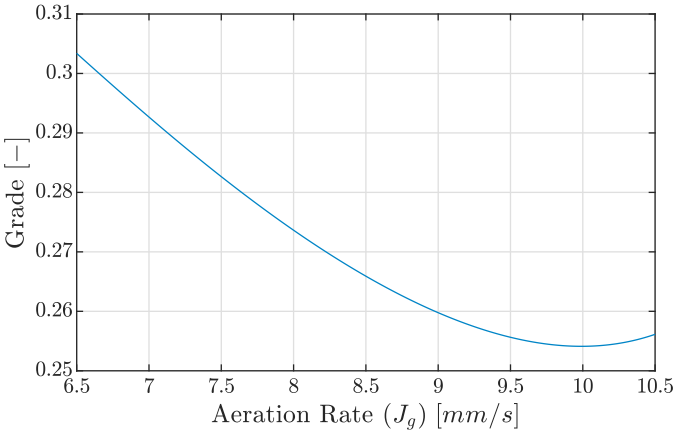

Fig. 4. Steady-state simulation of aeration rate and grade measured in the hopper.

5. EXTREMUM SEEKING CONTROL

ESC is a control approach that is used to optimise a system by maximising an objective function. The plant can be considered as a reference-to-output map that has an extremum which is the operating point where the objective function is maximised. When this map is unknown or contains uncertainty, it is necessary to use some sort of adaptation to find the extremum that maximises the output (Krstić and Wang, 2000). A perturbation-based ESC uses a slow periodic signal added to the input of the system to perturb the plant and steer the plant through the map towards the extremum. The controller adjusts the input based on the gradient extracted from the measured objective function as it changes due to the perturbations added to the input. The continuous perturbations allow the ESC to track an unknown time-varying optimum over time, even in the presence of external disturbances. One advantage of ESC is that the controller is model-free. Therefore, as long as the objective function has a maximum and is convex, the controller does not require any knowledge of the process to steer the process to the optimal operating point (Wang et al., 1999).

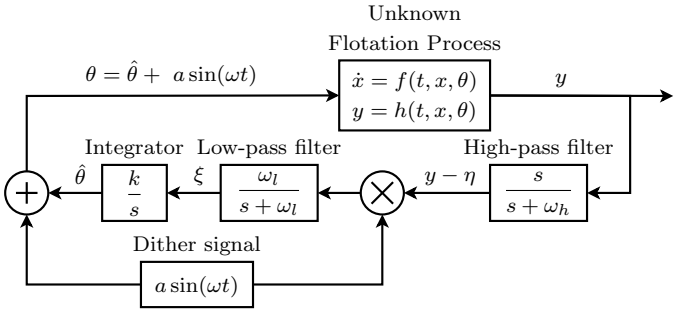

Fig. 6. Extremum seeking control scheme, reproduced from Krstić and Wang (2000).

Fig. 6 shows the peak seeking feedback scheme of a perturbation-based ESC. In the diagram, the flotation process is represented by the functions $\dot{x} = f(t,x,\theta)$ and $y = h(t,x,\theta)$. The process dynamics are unknown to the controller and the functions f and h are considered as unknown black-box functions that take an input, θ, and provide an output, y, which is the measured objective function. The dither signal is a slow periodic perturbation, $a\sin(\omega t)$, where a is the amplitude and ω is the perturbation frequency. The dither signal is added to $\hat{\theta}$, the best estimate of the optimal operating point (θ^*). The perturbations create a periodic response in the output which the high-pass filter isolates by removing the steady-state component from y, resulting in the filtered output, $y - \eta$. The periodic response in the output will either be in or out of phase with the dither signal depending on the location of $\hat{\theta}$ relative to θ^*. The product of $y - \eta$ and the dither signal contains the gradient, ξ, which is extracted with the low-pass filter. The sign of the gradient, ξ, provides the direction to the integrator for moving $\hat{\theta}$ towards θ^*. The integrator gain, k, controls how aggressive the ESC will be and has to be selected sufficiently small to ensure convergence (Krstić and Wang, 2000). The closed-loop system dynamics of Fig. 6 are summarised,

$$\dot{x} = f\left(t, x, \theta\right), \tag{16a}$$
$$y = h\left(t, x, \theta\right), \tag{16b}$$
$$\dot{\hat{\theta}} = k\xi, \tag{16c}$$
$$\dot{\xi} = -\omega_l \xi + \omega_l \left(y - \eta\right) a \sin\left(\omega t\right), \tag{16d}$$
$$\dot{\eta} = -\omega_h \eta + \omega_h y. \tag{16e}$$

For the ESC to operate effectively, the perturbation frequency has to be slow enough that the reference-to-output map of the plant appears as a static map. The static map ensures that the plant dynamics do not interfere with the ESC and that the controller can search along the static map for the optimum operating point. The system, therefore, has three time scales with sufficient separation between the scales. The fastest time-scale is the process dynamics of the plant together with the stabilising and regulatory controllers. The next time-scale is the periodic perturbations which have to be slower than the process dynamics. The slowest time-scale is the filters in the ESC scheme as the cut-off frequencies have to be lower than the frequency of the perturbation signal.

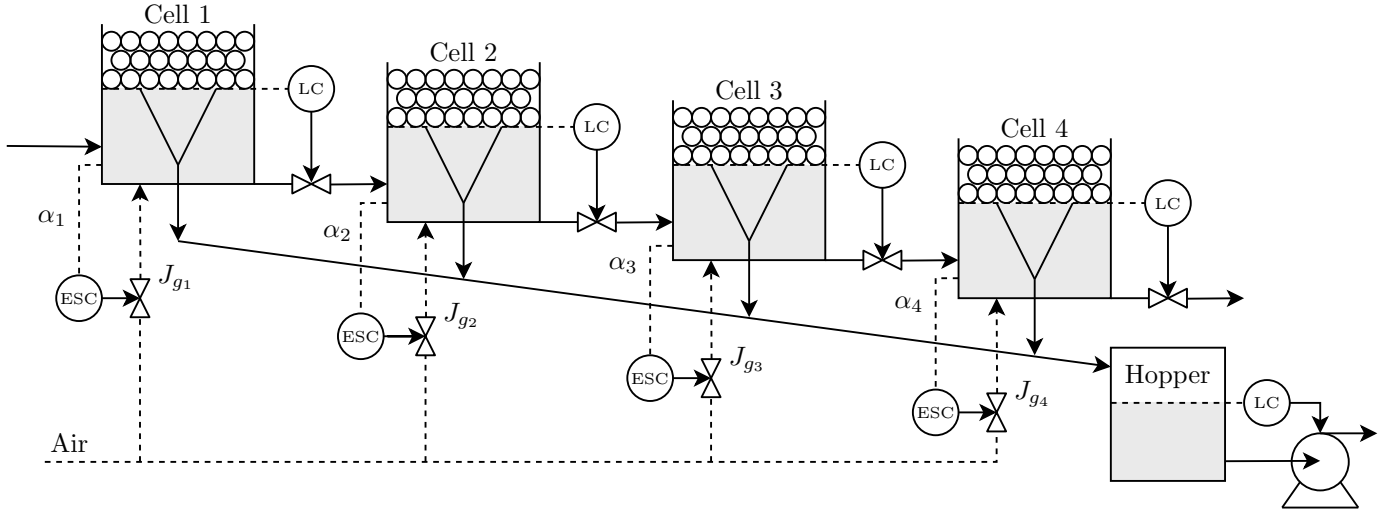

Fig. 5. Flotation circuit used in the simulation study with the implemented controllers.

6. SIMULATIONS AND RESULTS

The purpose of the simulations is to demonstrate how well the ESC works as an optimisation controller on a flotation circuit. Fig. 5 shows a diagram of the flotation cells and controllers implemented on the circuit. The flotation cells are modelled with the dynamic flotation model given in Section 3. On the tailings stream of each of the cells, as well as the outflow of the hopper, PI-controllers are implemented to stabilise the pulp levels (L_k). The levels are controlled to a setpoint while the froth height of each cell, h_{f_k}, is kept constant. A separate ESC is implemented on each of the cells to maximise the air recovery, α_k, by manipulating the aeration rate to the cells. The local optimisation problem of finding the aeration rate that produces the maximum air recovery can be solved in each of the cells independently of how the other cells are being operated. The ESCs are all tuned similarly with a relatively slow perturbation ($a\sin(\omega t)$). The tuning parameters, as given in Table 1, were chosen fairly conservatively to ensure convergence to the peak air recovery operating point.

Table 1. ESC parameters.

Parameter	Value	Unit
Dither amplitude (a)	0.001	
Dither frequency (ω)	25.13	rad/h
High-pass cut-off frequency (ω_h)	18	rad/h
Low-pass cut-off frequency (ω_l)	0.036	rad/h
Integrator gain (k)	250	

The simulation starts at a sub-optimal operating point and the ESC optimises the flotation circuit over a period of 10 days. After 10 days the plant is subjected to a large disturbance that changes the peak air recovery operating point significantly. In reality, the disturbances would most often be much smaller and more gradual. The disturbance was made by increasing $K_{\alpha_{J_{g0}}}$ in (9) by 1.6. Since the effect of individual specific disturbances like a change in mineral grade or percentage solids is not modelled, the step-change in $K_{\alpha_{J_{g0}}}$ aims to simulate any combination of disturbances that influence the optimal peak air recovery operating point. The total simulation time is 20 days to give the system enough time to stabilise at the optimal operating point. Fig. 7 show the simulation result of the air recovery and the aeration rate. Fig. 8 show the simulation result of the mineral grade and recovery and Fig. 9 show the grade-recovery curve.

7. DISCUSSION

The results in Fig. 7 show the air recovery and the aeration rate for the 20-day simulation period. The process starts at a sub-optimal operating point and the extremum seeking controller steers the process to the optimal operating point at the peak air recovery. Once the peak air recovery is reached in each of the cells, after around 5 days, the perturbations continue to keep the process at the optimal operating point. After 10 days when the simulated disturbance changes the peak air recovery point, the ESC can be seen to steer the flotation circuit towards the new

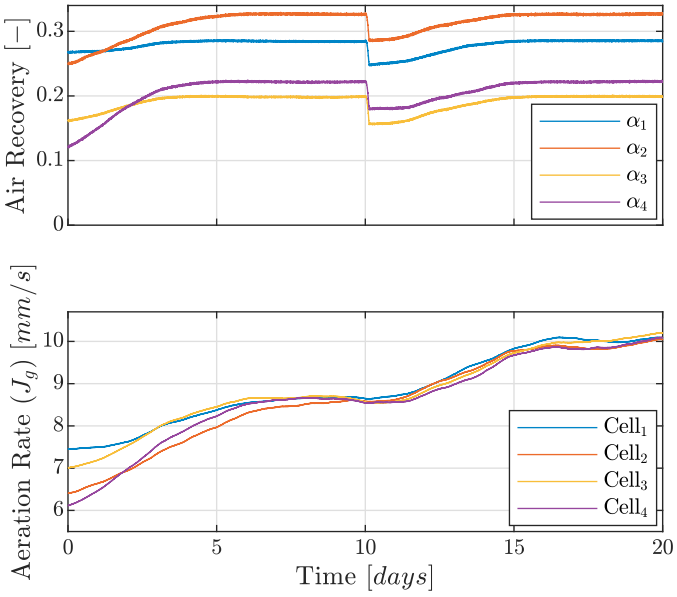

Fig. 7. Simulation result of air recovery (α_k) and aeration rate (J_{g_k}) for each of the four flotation cells.

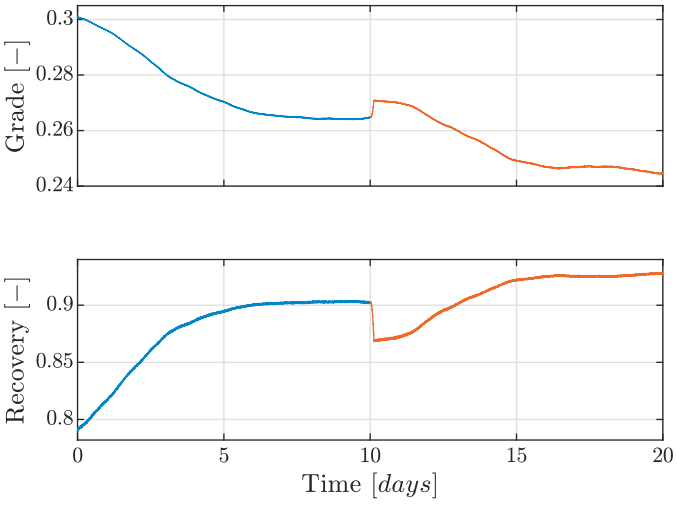

Fig. 8. Simulation result of grade and recovery measured in the hopper.

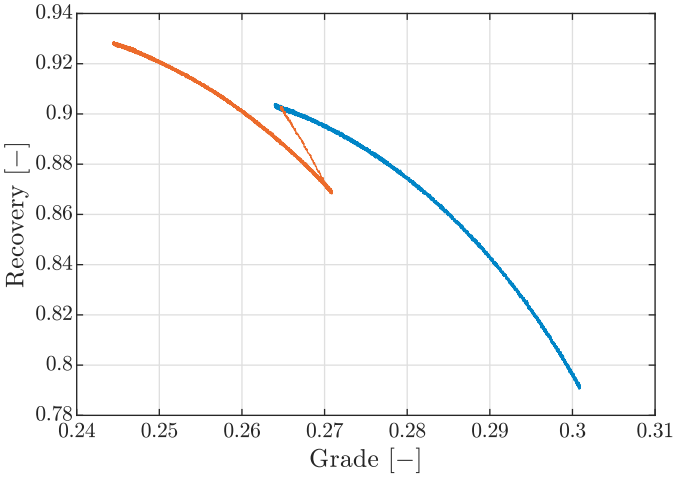

Fig. 9. Simulation result of grade-recovery curve.

peak air recovery operating point where the air recovery is once again maximised.

The extremum seeking controller increases the recovery up to 90.3% where it stabilises at the peak air recovery point. The theoretical maximum mineral recovery under these operating conditions is 90.66% as shown in Fig. 3. This increase in recovery comes at a cost of a reduced grade which drops to below 27%.

The grade-recovery operating point, shown in Fig. 9, moves from the bottom right at a high grade and low recovery towards the top left where the recovery is maximised at a reduced grade. At this point, the perturbations move the operating point back and forth over the curve to continually track the peak air recovery operating point. When the disturbance takes place, the curve changes and the process starts over, the new grade-recovery curve is the orange line to the left of the first curve in Fig. 9. Once again, the optimisation reduces the grade and increases the recovery up to 92.8%. The theoretical maximum mineral recovery under these new operating conditions is 93.14%.

8. CONCLUSION

The simulation shows that the ESC is able to manipulate the aeration rate to maximise the air recovery and maintain the process at the extremum. The ESC moves the flotation circuit from a suboptimal operating point to the point where the air recovery is maximised and the mineral recovery is optimised to within 0.4% of the theoretical maximum possible under the given operating conditions. After the simulated disturbance, the ESC once again reaches the peak air recovery operating point and maximises the mineral recovery to the same accuracy. The perturbation-based ESC scheme is model-free and does not need a plant model to optimise the plant. This is an important advantage since flotation models are often very complicated and difficult to fit to a plant.

There are also some potential disadvantages to ESC, the main one being that due to slow dynamics of the flotation circuit and slow perturbations, the optimisation is quite slow. If the peak air recovery operating point changes rapidly as shown in Phillpotts et al. (2020), the perturbation-based ESC would need to react faster. To mitigate this problem, the initial operating conditions must be selected closer to the optimum so that the ESC does not have to explore far to reach the extremum. The integrator gain can also be increased to speed up the convergence. However, this could result in increased sensitivity to noise. Another disadvantage is that the perturbations can be visible in the output and the process is never at a steady-state. Instead, it operates within the neighbourhood of the steady-state optimum. This could decrease the performance of the controller slightly, but if the perturbation amplitude is small enough the effect should be negligible. Finally, since air recovery measurements can be prone to errors, it may cause the ESC to operate the circuit at a different point from where true peak air recovery occurs.

In future work, the controller can be expanded to a multiple-input, single-output controller by manipulating the froth height as well as the aeration rate to further increase the air recovery. Future work can also focus on improving the convergence time of the optimisation by using a time-varying ESC approach (Guay and Dochain, 2015) or a non-gradient-based ESC (Nelder and Mead, 1965).

REFERENCES

Bergh, L.G. and Yianatos, J.B. (2011). The long way toward multivariate predictive control of flotation processes. *Journal of Process Control*, 21(2), 226–234.

Guay, M. and Dochain, D. (2015). A time-varying extremum-seeking control approach. *Automatica*, 51, 356–363.

Guay, M., Moshksar, E., and Dochain, D. (2015). A constrained extremum-seeking control approach. *International Journal of Robust and Nonlinear Control*, 25(16), 3132–3153.

Hadler, K. and Cilliers, J.J. (2009). The relationship between the peak in air recovery and flotation bank performance. *Minerals Engineering*, 22(5), 451–455.

Hadler, K., Smith, C.D., and Cilliers, J.J. (2010). Recovery vs. mass pull: The link to air recovery. *Minerals Engineering*, 23(11-13), 994–1002.

Krstić, M. and Wang, H.H. (2000). Stability of extremum seeking feedback for general nonlinear dynamic systems. *Automatica*, 36(4), 595–601.

Laurila, H., Karesvuori, J., and Tiili, O. (2002). Strategies For Instrumentation and Control of Flotation Circuits. *Mineral Processing Plant Design, Practice and Control*, 2, 2174–2195.

Nelder, J.A. and Mead, R. (1965). A simplex method for function minimization. *The Computer Journal*, 7(4), 308–313.

Oosthuizen, D.J., le Roux, J.D., and Craig, I.K. (2021). A dynamic flotation model to infer process characteristics from online measurements. *Minerals Engineering*, 167, 106878.

Phillpotts, D., Whitehead, B., and Ramatsoma, S. (2020). Monitoring of air recovery for froth flotation optimisation on an industrial circuit. *XXII International Mineral Processing Congress*, 3348–3357.

Quintanilla, P., Neethling, S.J., Navia, D., and Brito-Parada, P.R. (2021). A dynamic flotation model for predictive control incorporating froth physics. Part I: Model development. *Minerals Engineering*, 173, 107192.

Shean, B., Hadler, K., and Cilliers, J.J. (2017). A flotation control system to optimise performance using peak air recovery. *Chemical Engineering Research and Design*, 117, 57–65.

Shean, B.J. and Cilliers, J.J. (2011). A review of froth flotation control. *International Journal of Mineral Processing*, 100(3-4), 57–71.

Smith, C.D., Hadler, K., and Cilliers, J.J. (2010). Flotation bank air addition and distribution for optimal performance. *Minerals Engineering*, 23(11-13), 1023–1029.

Wang, H.H., Krstić, M., and Bastin, G. (1999). Optimizing bioreactors by extremum seeking. *International Journal of Adaptive Control and Signal Processing*, 13(8), 651–669.

Ziolkowski, L., le Roux, J.D., and Craig, I.K. (2021). Optimizing grinding mill performance using extremum seeking control. *IFAC-PapersOnLine*, 54(11), 43–48.